J Mater Sci (2017) 52:11168–11178

Macroporous Materials

Hierarchical macroporous–mesoporous γ-alumina monolithic green bodies with high strength

Andraž Kocjan[1,*], Thomas Konegger[2], and Aleš Dakskobler[3]

[1] Department for Nanostructured Materials, Jožef Stefan Institute, Ljubljana, Slovenia
[2] Institute of Chemical Technologies and Analytics, TU Wien, Getreidemarkt 9/164-CT, 1060 Vienna, Austria
[3] Vall-cer d.o.o., Tehnološki park 24, 1000 Ljubljana, Slovenia

Received: 31 December 2016
Accepted: 6 February 2017
Published online: 14 February 2017

ABSTRACT

Hierarchical macroporous–mesoporous alumina (HMMA) and hierarchical mesoporous alumina (HMA) monolithic green bodies were fabricated by cold isostatic pressing (CIP) of mesoporous alumina (MA) powder, which was prepared by a quick, facile and very pure synthesis route that involved exploitation of the naturally self-driven aluminum nitride powder hydrolysis. The hierarchically self-assembled, nanocrystalline, yet micron-sized MA powder exhibited a controlled porosity, a fine crystallite size, a relatively large surface area and large pore volumes. The textural characteristics of the MA powder were analyzed, while the effect of the consolidation pressure on the pore size evolution, mechanical and permeability properties of the consolidated HMMA and HMA monoliths were investigated. At the lowest CIP pressures, the HMMA monoliths possessed favorable permeability characteristics with Darcian permeability constants up to 2×10^{-15} m^2, also exhibiting a low thermal conductivity (≥0.185 W/mK), sufficient flexural strength (≥6 MPa) with an accessible porosity of ≤65%, a pore volume of ≤0.69 cm^3/g and a macropore opening diameter of ≤370 nm at a constant mesopore opening diameter of about 4.5 nm. Increasing the CIP pressure resulted in the shrinkage of the macropores and a consequent suppression of the permeability characteristics; however, the flexural strength of the HMA monolith CIPed at 800 MPa increased to 51 MPa, which is the highest reported strength for a dry-pressed, binderless ceramic green body with an accessible porosity of 42% and a theoretical density of 44.3%.

Introduction

Mesoporous alumina (MA) is nowadays heavily exploited due to its fine particle size, controlled porosity, large surface area and the catalytic activity of its surfaces, finding applications in industry as adsorbents, catalysts or catalyst carriers, membranes for filtration, binders, coatings, soft abrasives, etc. [1]. Recently, the potential use of MA in medicine as biomaterials with increased osteoblast cytocompatibility properties, or as carriers and adjuvants, was

Address correspondence to E-mail: a.kocjan@ijs.si

DOI 10.1007/s10853-017-0894-z

also recognized [2, 3]. MA is derived from aluminum (oxi)hydroxides (γ-AlOOH; Boehmite) obtained by topotactic dehydration/decomposition, meaning the crystallographic orientations between the precursor and the product are defined and reproducible. In this way, the evolved texture and porosity of the MA, along with the temperature of the transitions taking place are influenced by the nature of the boehmite precursor [1, 4, 5].

In the case of catalyst supports, porous electrodes, sorption and/or separation, the incorporation of macropores (>50 nm) into mesoporous (2 ± 50 nm) MA monoliths, yielding hierarchical macroporous–mesoporous aluminas (HMMAs) [6–13] offers a promising strategy to minimize the diffusion barriers and potentially enhances the distribution of active sites [14]. For example, if some fluid has to be introduced into the monolith, macropores ensure a high fluid permeability, while the mesopores (and micropores) are the ones on which separation, activation and/or degradation occur. The introduction of macropores, however, should not deteriorate the mechanical properties. However, the fabrication of HMMA monoliths is currently still a challenging process. The synthesis strategies to obtain MA precursor require either the use of alkoxides (sol–gel) and organic solvents or complex and multiple-step aqueous synthesis routes, both relying on lengthy aging and calcinations treatments. The aqueous approach is based on the neutralization of aluminum salts and thereby requiring extensive washing, since the cationic and anionic species as side-product impurities limit the control of the precipitates' morphology [1, 15]. Both methods may employ various complex and hazardous surfactants as structure-directing agents, while the sol–gel route also requires other organics for the purpose of gelation initiation and phase separation. In addition to the complex synthesis strategies and limited amounts of obtained MA precursor, the degree of agglomeration and the particle size distribution are rarely presented and discussed, which are also important final properties that ultimately determine its further industrial applicability. On the other hand, the macropores are commonly introduced to MA via replica techniques using sacrificial templates, which then need to be eliminated, i.e., burned out during the slow and controlled calcination step. Moreover, except for the surface properties, other important properties of synthesized HMMA monoliths, such as mechanical, thermal and permeability characteristics, are often not presented.

In the present paper, we report on a quick, facile and very pure synthesis path for the preparation of hierarchically self-assembled, nanocrystalline, yet micron-sized, high surface area, MA powders, exhibiting controlled porosity, a fine crystallite size, relatively large surface area and pore volumes. It is based on the naturally self-driven aluminum nitride (AlN) powder degradation in aqueous environments, i.e., hydrolysis, where our recent in-depth studies of the solid reaction products of the AlN powder hydrolysis [16, 17] along with its reaction kinetics [18] made it possible for us to develop an innovative synthesis of MA powders. Previously, we exploited it in the hydrolysis-assisted solidification (HAS) of ceramic suspensions for the processing of high-performance porous alumina ceramics [19] and for the synthesis of nanostructured alumina coatings with a large surface area [20–22]. Here, we show how high-performance HMMA and HMA monolithic green bodies can be fabricated simply by the dry consolidation of hydrolysis-derived MA powders via cold isostatic pressing (CIP), not requiring any post-calcination treatment. The characteristics of the synthesized MA powder were inspected, and the effect of the consolidation pressure on the pore size evolution, mechanical and permeability properties of the consolidated HMMA and HMA monoliths were carefully investigated.

Materials and methods

Sample preparation

The mesoporous, γ-alumina (MA) powder was synthesized by hydrolyzing the AlN powder in a diluted aqueous suspension. For this purpose, AlN Grade C (H.C. Starck, Berlin, Germany) with a nominal particle size of 1.2 μm was used. A mass of 3 wt% of AlN powder was dispersed in deionized water preheated to 95 °C. The suspension was then placed in an oven that was heated to 120 °C, where the hydrolysis took place. After 4 h of hydrolysis, the suspension was filtered, washed with 2-propanol (Sigma-Aldrich GmbH, Taufkirchen, Germany) and air-dried at 150 °C for 2 h. The as-obtained MA powder was calcined in a resistance oven in dry air at 500 °C at a heating rate of 10 °C/min, with a dwell time of 1 h at

the final temperature. The hierarchical mesoporous–macroporous alumina (HMMA) and hierarchical mesoporous (HMA) alumina monolithic green bodies were fabricated by dry consolidation of the MA powder. Prior to consolidation, the powder was held at 150 °C in an oven. The initial uniaxial dry-pressing in a 20-mm steel die at 50 MPa was followed by a subsequent CIP using final pressures of 100, 200, 400, 600 and 800 MPa.

Characterization

Laser particle-size analyzer (LA-920, Horiba, Kyoto, Japan) was employed for the particle size measurement of the synthesized MA powder. Prior to dispersion of the MA powder in deionized water, 3-basic ammonium citrate was used as a stabilizing agent. The pH was simultaneously established to a value of 8.5. The measurement was conducted after 5 min of stirring and ultra-sonication of the suspension in the sample cell. Scanning (SEM; JSM-7600F, Jeol, Tokyo, Japan) and transmission (TEM; JEM 2100, Jeol, Tokyo, Japan) electron microscopy imaging was used to evaluate the morphology of the MA powder. A microstructural analysis of the consolidated HMMA monolithic samples was performed with SEM at an accelerating voltage of 5 kV. Prior to the investigation, the surfaces of the monoliths were ion-beam polished using an SM09010-CP ion-beam polisher (Jeol, Tokyo, Japan), where argon was used as the source of the ions at 5 kV. X-ray diffraction (XRD) patterns of the MA powders prior to consolidation were recorded using a PANalytical X'pert PRO MPD diffractometer (Almelo, Netherlands) equipped with a PIXcel detector and using a Cu–$K_{\alpha 1}$ radiation source. The measurements were taken using fixed divergence (1°) and anti-scattering slits, a 10-mm mask, a continuous scan mode in the 2θ range 10°–75°, with a step size of 0.00656° and a scan speed of 0.01113°/s. Nitrogen adsorption/desorption isotherms were recorded at liquid nitrogen temperature using a nitrogen sorption analyzer (Quantachrome, Nova 2000e). The samples were degassed at 250 °C in a vacuum for 16-h prior to the measurement. The surface area was calculated with the Brunauer–Emmett–Teller (BET) equation using the nitrogen adsorption data in the P/P_0 range between 0.05 and 0.3 (7-point analysis), and the pore size distribution, pore volume and average pore size were extracted from the desorption branch of the isotherm using the Barrett–Joyner–Halenda (BJH) method. The pore volume and the pore size distribution of the HMMA and MA monoliths were determined using a Pascal series mercury intrusion porosimeter (Thermo Scientific) within the pore size (diameter) interval 3.2 nm to 50 μm. The surface tension and the contact angle of the mercury were set to 0.485 mN/m and 130°, respectively. The effective thermal conductivities of the samples were measured with a hot disk thermal constant analyzer TPS 2500 s (HotDisk AB, Gothenburg, Sweden), where two CIPed monolithic green bodies in the form of cylinders with a minimum height and diameter of 4 and 16 mm, respectively were used for the measurement. A 6.4-mm hot disk sensor was used. The measurement parameters were set to 100 mW output power and 40 s measuring time, which resulted in a temperature increase in about 3 °C. An average value with a standard deviation was calculated from six measurements per sample with a 45-min conditioning time between each measurement. More details can be found elsewhere [23]. The biaxial flexural strengths were measured with a piston-on-three-balls setup, according to the ISO 6872 standard, on a universal testing machine (Quasar 100, Galdabini, Cardano al Campo, Italy) at a loading rate of 1 mm/min. For each test, at least 3 samples were fractured, from which the average strengths and standard deviations were calculated. The permeability testing was conducted at room temperature using cylindrical samples with a diameter of 18–20 mm and a thickness of 3 mm, with filtered compressed air as the fluid. The test setup was constructed on the basis of DIN EN ISO 4022 in order to achieve unidirectional, axial flow through the specimen. A concentric sealing geometry facilitated the prevention of radial flows, thus minimizing the errors caused by radial pressure differentials within the specimen volumes being tested. The permeated area A was 84 mm^2. Using a soap-bubble flow meter, the stationary permeating gas flow Q was recorded as a function of the differential pressure between the upstream and downstream sides of the specimen, varying Δp between 0.25 and 3 bar. Initially, a screening of the permeability behavior as a function of cold isostatic compaction pressure was conducted using individual samples (CIP150–CIP800). The poor mechanical properties of the CIP100 rendered permeability testing of these samples impossible. Subsequently, batches CIP150 and CIP200 were tested in more detail, recording between 8 and 12 sets of

pressure drop and Q values per sample, with three samples tested per batch. Using Forchheimer's equation for compressible fluids [1], the Darcian (k_1) and non-Darcian permeabilities (k_2) were evaluated, with p_i and p_o being the absolute pressures on the upstream and downstream sides, respectively, and assuming an air viscosity of $\eta = 1.84{\cdot}10^{-5}$ Pa·s and an air density of $\rho = 1.16$ kg m^{-3} ($p_o = 990$ mbar and T = 22 °C), Eq. 1:

$$\frac{p_i^2 - p_o^2}{2p_o \cdot l} = \frac{\eta}{k_1}\frac{Q}{A} + \frac{\rho}{k_2}\left(\frac{Q}{A}\right)^2 \quad (1)$$

k_1 and k_2 were calculated by fitting a quadratic function to (p_i^2-$p_o^2/2p_o l$) versus Q/A using the least-squares method.

Results and discussion

Hydrolysis-derived MA powder

For the synthesis of the boehmite precursor (B; γ-AlOOH), the hydrolysis of the AlN powder was exploited, which turns out to be an extremely facile synthesis procedure that does not require any hazardous solvents, salts or surface-active agents, nor lengthy hydrothermal treatments. The kinetics and aluminum hydroxide evolution are strongly dependent on the starting temperature and pH of the suspension [17, 24]. The hydrolysis and aging of the diluted aqueous AlN powder suspension containing 3 wt% of solids, which was kept boiling for 4 h, resulted in a complete degradation and transformation of the AlN particles to a well-crystallized γ-AlOOH phase, as shown in Fig. 1. After calcination at 500 °C for 1 h, the γ-AlOOH was topotactically transformed into the γ-Al_2O_3 phase. During the topotactic transformation, a slight structural collapse of the γ-AlOOH occurs due to the dehydration process, followed by an aluminum migration process occupying tetrahedral and octahedral sites. The outcome of the process is that the morphological and textural properties remain related to the nature of the starting hydroxide [5, 25, 26]. The Scherrer equation was used to obtain an estimate of the primary crystallite sizes [27]. The calculation of the average crystallite size was based on $(010)_B$ and $(100)_{MA}$ diffraction peaks for γ-AlOOH (B) and γ-Al_2O_3 (MA), respectively. The calculated $d_{(010)B}$ and $d_{(100)MA}$ were

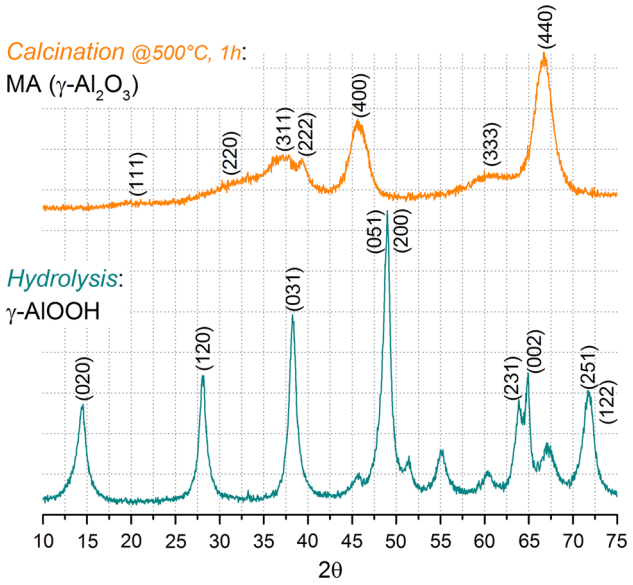

Figure 1 XRD patterns of the as-synthesized MA precursor (γ-AlOOH) via the hydrolysis of AlN powder and the obtained MA powder (γ-Al_2O_3) after calcination at 500 °C for 1 h.

7 and 4 nm, respectively, indicating the nanocrystalline nature of the powders.

The SEM micrograph of the as-prepared MA powder is shown in Fig. 2a. The powder is in the form of micron-sized bundles of agglomerated nanocrystalline 2D lamellas, or nanosheets, forming flower-like structures. Such structures are indicative of a hierarchical self-assembly, which is operating during the AlN powder hydrolysis process [28]. The benefit of hierarchical self-assembly is to ease the processing of nanostructured powders, since their arrangement into hierarchical, micron-sized entities, while retaining their intrinsic "nano" features makes them environmentally friendlier (less hazardous) and easier to handle and recollect [29]. The AlN-hydrolysis-based synthesis employed permits the preparation of abundant amounts of the MA powder, which exhibits beneficial flowability characteristics, similar to granulated powders and can be easily re-dispersed. The particle size distribution was determined (Figure S1, Supplementary information). The distribution was narrow and monomodal in type with a d_{mean} of about 7 μm. On the other hand, d_{10}, d_{50} and d_{90} were 3.7, 6.05 and 9.2 μm, respectively. A closer inspection of the lamellar morphology of the powder using TEM analyses reveals the nanocrystalline nature of the otherwise micron-sized MA powder. From Fig. 2b, the thickness of a single 2D nanosheet was

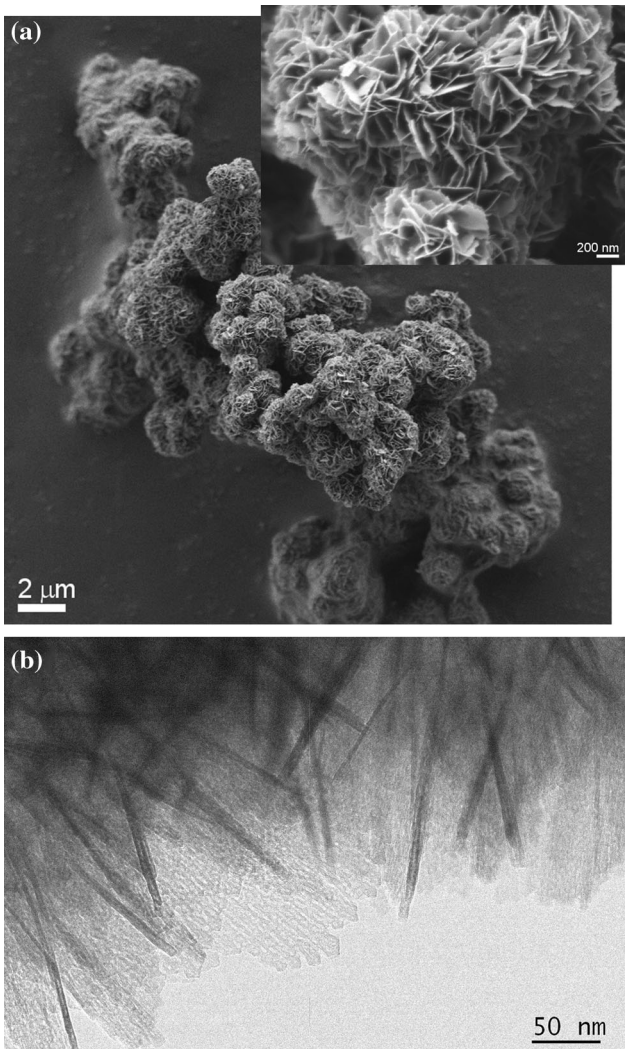

Figure 2 **a** Scanning and **b** transmission electron micrographs of AlN powder hydrolysis-derived self-assembled MA precursor powder.

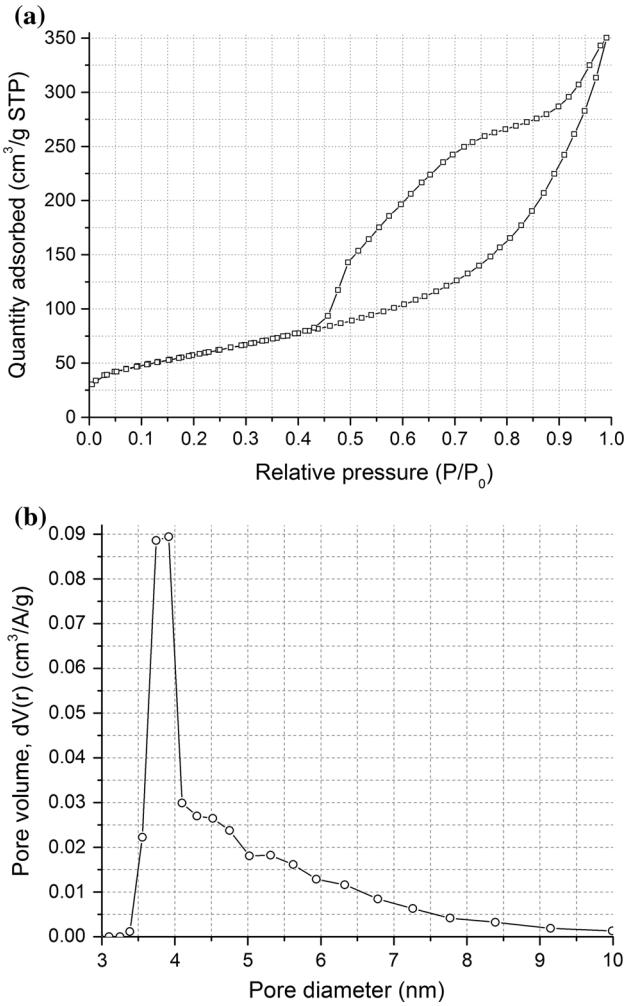

Figure 3 **a** Nitrogen adsorption–desorption isotherm and **b** the isotherm-derived pore size distribution for the hydrolysis-derived MA powder calcined at 500 °C for 1 h.

estimated to be 6.6 nm, which is slightly more than the estimation based on the Scherrer equation from the XRD analysis (Fig. 1), where the value should be slightly underestimated due to the instrumental broadening. In addition, the homogeneously distributed mesopores are also clearly visible, confirming the mesostructured nature of the as-prepared γ-Al_2O_3 also facilitating the increased specific surface area and pore volume. Similar structures have been prepared previously via the neutralization of aluminum salts, but at the expense of requiring hydrothermal or microwave-assisted synthesis and extensive washing [30–32].

The typical nitrogen adsorption–desorption isotherm of the MA powder calcined at 500 °C plotted in Fig. 3a exhibits type-IV isotherms according to the IUPAC classification, which is representative of mesoporous materials. The textural properties of the MA powder derived from the isotherm reveal a relatively high mesopore volume of 0.64 $cm^3 \cdot g^{-1}$ and a BJH pore diameter of 3.9 nm, being slightly above the 2-nanometre border between the micro- and mesoporosity classifications. The BET specific surface area was 207 m^2/g. The BJH pore size distribution presented in Fig. 3b is indicative of a narrow pore size distribution. The majority of the pores are concentrated in the diameter range 1.6–4.5 nm. The distribution seems to be of the multimodal type with three mean pore diameters. The first and most intense is around 1.9 nm, while the second and third ones are at 2.3 and 2.7 nm, respectively.

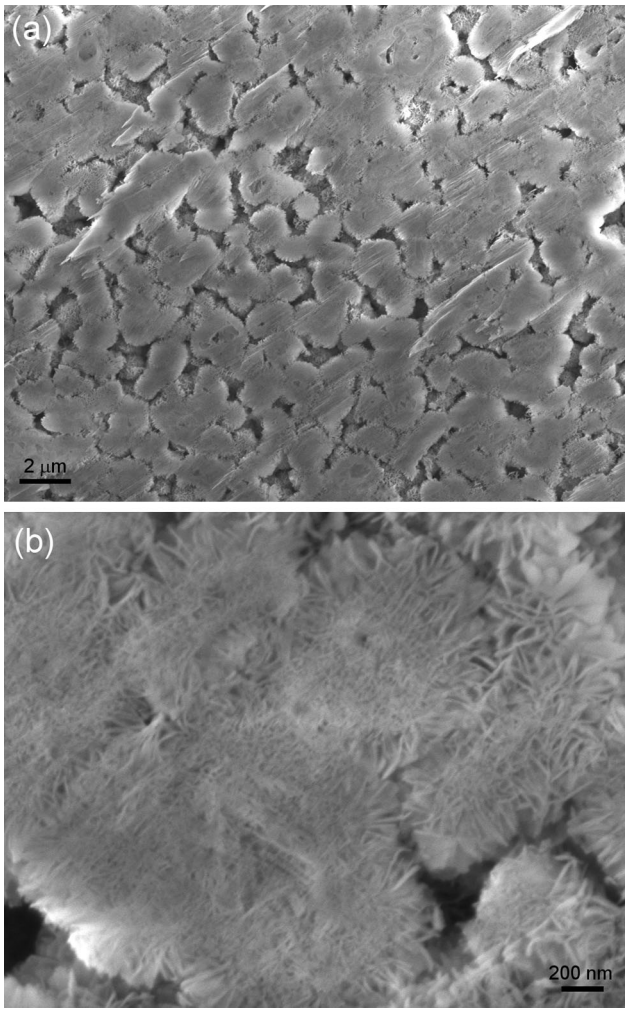

Figure 4 **a** Lower- and **b** higher-magnification scanning electron micrographs of an ion-polished HMMA monolith consolidated at 100 MPa of CIP pressure.

Consolidated HMMA and HMA monoliths

Consolidation and structuring

The as-synthesized, hydrolysis-derived hierarchically self-assembled MA powder exhibited excellent powder flowability characteristics and consolidation behavior in the absence of binders and plasticizers. It was consolidated and structured simply by dry compaction, i.e., CIPing, to yield HMMA and HMA monolithic green bodies in the form of pellets, where the CIP pressure was varied from 100 to 800 MPa. Figure 4a shows an SEM micrograph of the ion-polished surface of the HMMA monolithic green body CIPed at 100 MPa. The micrograph is indicative of the enhanced consolidation ability of the MA powder, where micron-sized, agglomerated lamellar bundles (Fig. 2) were brought into close contact. The diameter of the bundles is about 1–2 microns in size. The enhanced consolidation resulted in the formation of homogeneously distributed macropores throughout the green body, which are also around 1–2 microns in size. The higher-magnification SEM micrograph (Fig. 4b) reveals a controlled demolition of the hierarchical structures, where the 2D lamellar nanosheets found in the larger macropores remain intact, while when in contact, they provide mechanical interlocking. In the middle of the micron-sized bundles, the loosely packed, primary crystallites form a mesoporous core structure of the HMMA monolith.

The CIP consolidation pressure dependence of the as-formed HMMA and HMA monolithic green bodies on the density, porosity, pore volume, and evolution of the pore opening diameter was analyzed using mercury intrusion porosimetry. The data are presented in Table 1. All the parameters increase and/or decrease almost linearly with an increase in the consolidation pressure. Increasing the CIP pressure from 100 to 800 MPa resulted in a density increase in the HMMA and HMA monoliths from 0.94 to 1.51 g/cm^3, which roughly corresponded to an increase in the relative density from 27.6 to 44.3%. On the other hand, the porosity and pore volume decrease from 65 to 42% and 0.69 to 0.28 cm^3/g, respectively. The as-prepared HMMA is highly porous, since it exhibits half or more open, accessible pores up to 600 MPa of CIP consolidation pressure.

Table 1 Bulk density, pore volume and porosity as a function of the CIP consolidation pressure extracted from mercury intrusion analyses for the HMMA and HMA monolithic green bodies

CIP (MPa)	Density (g/cm^3)	Porosity (%)	Pore volume (cm^3/g)
100	0.94 (27.6%[a])	65	0.69
200	1.05 (30.8%[a])	59	0.55
400	1.22 (35.8%[a])	54	0.36
600	1.40 (41.1%[a])	45	0.31
800	1.51 (44.3%[a])	42	0.28

[a] Calculated relative density when 3.41 g/cm^3 was taken as theoretical one

The pore volumes, especially in the case of 100 and 200 MPa of CIP pressure are also very high for monolithic green bodies, retaining the initial textural characteristics of the precursor MA powder.

The hierarchical meso–macropores size evolution is presented in Fig. 5, where the pore (opening diameter) size distribution (PSD) as a function of the consolidation CIP pressure from the mercury intrusion measurements is presented. The increase in CIP consolidation pressure governs the PSD. At the lowest pressures of 100–400 MPa, the green bodies exhibit hierarchical mesoporous–macroporous characteristics possessing a monomodal distribution of mesopores with d_{mean} positioned at approximately 4.5 nm, which corroborates well with the textural results obtained from nitrogen adsorption. The difference is in the amount and the size of the opening diameter of the macropores, when the HMMA monolithic green body was CIPed at lower pressures. The 100 MPa sample possesses more of the larger (d_{mean}) macropores compared to the 200 and 400 MPa samples, i.e., 370 versus 270 and 120 nm, respectively. With a further increase in the CIP consolidation pressure, the macropores shrink even more, becoming the larger fraction of hierarchical mesopores (labeled HMA instead of HMMA). Consolidating the MA powder at the highest CIP pressures of 600 and 800 MPa resulted in HMA bodies with a bimodal PSD with larger fraction of mesopores at 44 and 25 nm, respectively. The as-formed green bodies obtained via the dry consolidation route exhibit a superior primary crystallite packing, resulting in green densities far exceeding 40% of theoretical density, which, for example, is significantly higher compared to slip casting, which is a wet colloidal approach [33].

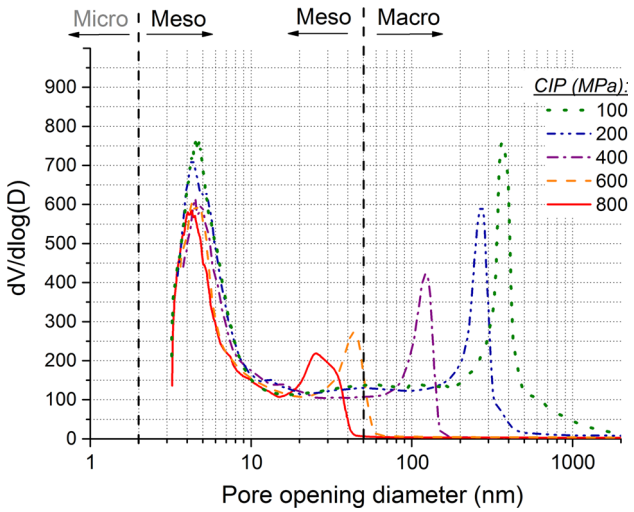

Figure 5 Pore (opening diameter) size distribution of the HMMA and HMA monoliths consolidated at different CIP pressures.

Thermal and mechanical properties

Thermal and mechanical properties of porous ceramic materials are important for their applicability. Therefore, the influence of the PSD evolution in terms of the consolidation CIP pressure on the thermal conductivity and flexural strength of the HMMA and HMA green monoliths were investigated, and the results are presented in Fig. 6. The nanosized primary crystallites and the large number of hierarchically distributed meso- and macropores present in the HMMA and HMA samples were indicative of the increased insulating properties. It is known that the thermal conductivity of the ceramics not only depends on the porosity level, but it is significantly influenced by the pore size-dependent phonon scattering [34] and the crystallite size-dependent interfacial thermal resistance [35], especially for crystallites smaller than 100 nm, as in the present case. The combination of homogeneous 5-nm-size primary crystallite packing (Fig. 2) in combination with the high pore volume of the meso- and macropores present in the HMMA consolidated monoliths at the lowest CIP pressure of 100 MPa resulted in an effective thermal conductivity that is slightly lower than 0.190 W/m·K. With higher pressures, the conductivity increased almost linearly, corresponding to the increase in density (and decrease in porosity),

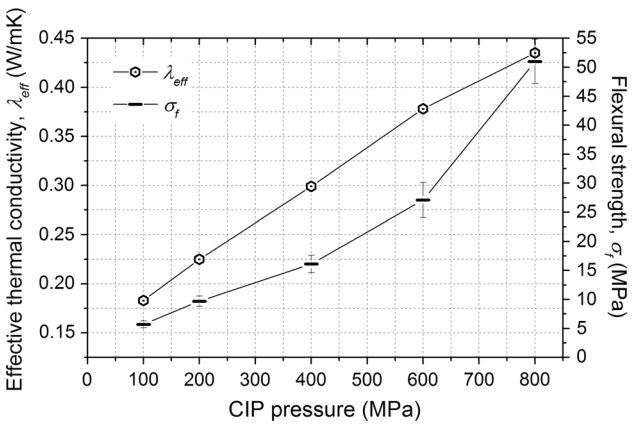

Figure 6 Effective thermal conductivity and flexural strength as a function of consolidation CIP pressure for the HMMA and HMA monolithic green bodies.

reaching 0.435 W/m·K at the highest CIP pressure of 800 MPa.

The mechanical properties of the green bodies produced from consolidated MA powder in terms of flexural strength were evaluated in order to check the beneficial contribution of the unique evolution of the microstructure, i.e., the presence of hierarchical macro–mesoporosity, combined with the homogeneous packing of the primary crystallites as well as the 2D nanosheet-like secondary particle interlocking as a result of the consolidation of the MA powder via CIPing. The HMMA samples consolidated at 100 and 200 MPa containing the largest fractions of macropores and consequently the lowest densities (Table 1), as expected, exhibited the lowest flexural strength of about 6 and 10 MPa, respectively. It then steadily increased with the increasing CIP pressure, reaching 16.2 and 27.5 MPa for 400 (HMMA) and 600 MPa (HMA) samples, respectively. At the highest pressure, the flexural strength reached a remarkable 51 MPa. Tensile strengths of several MPa were already achieved in green bodies; however, in samples prepared via colloidal pressure filtration [36] and/or the dry-pressing of granulated powders containing binders [37], all possessed significantly higher densities (lower porosities). Higher strengths in porous alumina ceramics of several tens of MPa were only achieved when partial sintering was employed. In addition, preliminary measurements of the hardness and elastic modulus for the 800-MPa sample were taken, obtaining 0.69 and 21 GPa, respectively. The values are coincidently very similar to those measured for bone [38], advocating such a shaping approach as a new possibility in the future mimicking of structuring of biomaterials. Similar properties were attained when vanadia nanoparticles were self-assembled by the evaporation of colloidal suspension to form a thin paper. The increased mechanical properties measured with a nanotensile tester were ascribed to hydrogen bond-reinforced nanoparticle assemblies [39]. In our case, however, we assume that homogenous dense packing of the primary crystallites provides arrays of stacked crystallites held together by Van der Waals forces. Future TEM work is planned, where we will systematically study the stress–strain behavior and fracture toughness coupled with detailed TEM analysis in order to better understand the increased mechanical strength of HMMA- and HMA-consolidated green bodies.

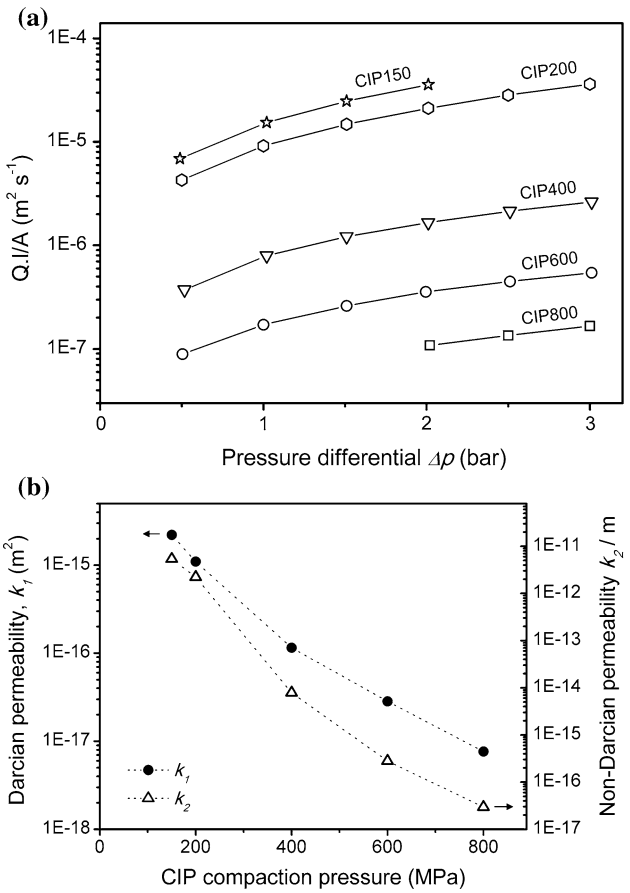

Figure 7 **a** Specific air flow through specimens versus pressure differential for HMMA monoliths consolidated at CIP pressures of 150[a], 200, 400, 600 and 800[b] MPa and **b** Darcian and non-Darcian permeabilities for HMMA monoliths consolidated at CIP pressures of 150, 200, 400, 600 and 800 MPa ([a]Rupture occurred at $\Delta p > 2$ bar; [b]exceedingly low flow rates at $\Delta p < 2$ bar).

Permeability characteristics

Finally, the permeability characteristics of the HMMA and HMA green bodies were evaluated and are presented in Fig. 7. Initial screening results of the permeability behavior of specimens showed a strong decrease in gas flow with the increasing CIP consolidation pressure, and specific air flows spanning several orders of magnitude (Fig. 7a). Accordingly, both Darcian and non-Darcian permeabilities, corresponding to the viscous and inertial contributions as given in Forchheimer's equation (Eq. 1), were found to correlate with the CIP pressure (Fig. 7b). An in-depth evaluation with an increased number of pressure drop and gas flow sets and multiple samples was conducted for batches CIP150 and CIP200 owing to their favorable permeability characteristics. A

Table 2 Summary of air permeability characteristics of porous specimens

CIP pressure (MPa)	No. of samples	k_1 (10^{-16} m^2)	k_2 (10^{-15} m)
150	3	22.1 ± 1.0	5390 ± 760
200	3	11.0 ± 0.6	2210 ± 450
400	1	1.15	7.86
600	1	0.284	0.281
800	1	0.076	0.030

Sample batches at CIP pressures of 150 and 200 MPa were tested in triplicate; hence, both mean and standard deviation are listed

quadratic relationship between the pressure drop and the gas velocity Q/A clearly indicates the presence of non-Darcian contributions (Figure S2, Supplementary information), thus justifying the use of Forchheimer's relation for permeability calculations in the recorded parameter range. The relative deviations of the permeability values between individual samples were found to be in the range of 5% for k_1 and up to 20% for k_2, thus demonstrating a good reproducibility of the permeability characteristics, in particular for the Darcian permeability k_1. An overview of the permeability data for screening and in-depth testing is listed in Table 2. Permeability characteristics significantly decreased at higher compaction pressures. For specimens consolidated at 150 and 200 MPa, Darcian permeabilities in the range of 10^{-15} m^2 and above were observed. As expected, owing to the pronounced mesopore structure, these values are well below the permeabilities encountered for porous ceramics with pore sizes in the μm range [40]. However, they can be considered adequate for a variety of applications in the fields of catalysis or separation, e.g., being in the same permeability range as structures proposed as membrane supports [41].

Conclusions

The naturally self-driven AlN powder hydrolysis was exploited for a quick, facile and very pure synthesis for the preparation of abundant amounts of hierarchically self-assembled, nanocrystalline, yet micron-sized, mesoporous alumina (MA) powder with fine crystallite size, controlled porosity, a relatively large surface area and pore volume, not needing any surfactants nor lengthy aging or the hydrothermal treatments. The MA powder is easily dispersible and possesses excellent flowability characteristics similar to granulated powders and is thus suitable for dry consolidation. Using cold isostatic pressing, hierarchical macroporous–mesoporous alumina (HMMA) green monoliths were obtained, exhibiting a low effective thermal conductivity and a relatively high flexural strength, retaining the favorable textural properties from the MA powder, and also showing promising permeability characteristics with Darcian permeabilities exceeding 10^{-15} m^2. Increasing the CIP consolidation pressure above 400 MPa resulted in the shrinkage of the macropores obtaining hierarchical mesoporous alumina (HMA) at the expense of deprivation of the permeability characteristics. However, the flexural strength at the highest CIP pressure of 800 MPa increased to 51 MPa having an accessible porosity of 42%, which is the highest reported strength value for an unsintered, porous green body. The resultant powder consolidation route not only has the potential for a controlled preparation of HMMA and HMA monoliths from hierarchically self-assembled powders, but through homogenous, dense packing of the primary crystallites, it has the potential to be suitable as a superior nanomaterials-structuring strategy not needing any thermal treatment in the field of processing science and technology for porous engineered and (bio)materials.

Acknowledgements

Slovenian Research Agency is acknowledged for funding the research program Engineering and Bioceramics (P2-0087). The authors are grateful to Darko Eterovič for the specimen preparation and mechanical testing.

Electronic supplementary material: The online version of this article (doi:10.1007/s10853-017-0894-z) contains supplementary material, which is available to authorized users.

References

[1] Euzen P, Raybaud P, Krokidis X et al (2002) Alumina. In: Schüth F, Sing K, Weitkamp J (eds) Handbook of porous solids. Wiley-VCH, Weinheim, pp 1591–1677

[2] Webster TJ, Hellenmeyer EL, Price RL (2005) Increased osteoblast functions on theta + delta nanofiber alumina. Biomaterials 26:953–960. doi:10.1016/j.biomaterials.2004.03.040

[3] Maquieira Á, Brun EM, Garcés-García M, Puchades R (2012) Aluminum oxide nanoparticles as carriers and adjuvants for eliciting antibodies from non-immunogenic haptens. Anal Chem 84:9340–9348. doi:10.1021/ac3020998

[4] Levin I, Brandon D (1998) Metastable alumina polymorphs: crystal structures and transition sequences. J Am Ceram Soc 81:1995–2012

[5] Iler R (1961) Fibrillar colloidal boehmite; progressive conversion to gamma, theta, and alpha aluminas. J Am Ceram Soc 44:618–624

[6] Deng W, Toepke MW, Shanks BH (2003) Surfactant-assisted synthesis of alumina with hierarchical nanopores. Adv Funct Mater 13:61–65. doi:10.1002/adfm.200390007

[7] Ren TZ, Yuan ZY, Su BL (2004) Microwave-assisted preparation of hierarchical mesoporous-macroporous boehmite AlOOH and γ-Al2O3. Langmuir 20:1531–1534. doi:10.1021/la0361767

[8] Zhang K, Fu Z, Nakayama T, Niihara K (2012) Structural evolution of hierarchically macro/mesoporous Al2O3 monoliths under heat-treatment. Microporous Mesoporous Mater 153:41–46. doi:10.1016/j.micromeso.2011.12.014

[9] Li L-L, Duan W-T, Yuan Q et al (2009) Hierarchical γ-Al2O3 monoliths with highly ordered 2D hexagonal mesopores in macroporous walls. Chem Commun 41:6174–6176. doi:10.1039/b912495k

[10] Tokudome Y, Fujita K, Nakanishi K et al (2007) Synthesis of monolithic Al2O3 with well-defined macropores and mesostructured skeletons via the sol–gel process accompanied by phase separation. Chem Mater 13:3393–3398. doi:10.1021/cm063051p

[11] Passos AR, Pulcinelli SH, Briois V, Santilli CV (2016) High surface area hierarchical porous Al $_2$ O $_3$ prepared by the integration of sol–gel transition and phase separation. RSC Adv 6:57217–57226. doi:10.1039/C6RA11477F

[12] Xu G, Li J, Cui H et al (2015) Biotemplated fabrication of porous alumina ceramics with controllable pore size using bioactive yeast as pore-forming agent. Ceram Int 41:7042–7047. doi:10.1016/j.ceramint.2015.02.007

[13] Bian S-W, Zhang Y-L, Li H-L et al (2010) γ-Alumina with hierarchically ordered mesopore/macropore from dual templates. Microporous Mesoporous Mater 131:289–293. doi:10.1016/j.micromeso.2010.01.004

[14] Parlett CMA, Wilson K, Lee AF (2013) Hierarchical porous materials: catalytic applications. Chem Soc Rev Chem Soc Rev 42:3876–3893. doi:10.1039/c2cs35378d

[15] Henry M, Jolivet JP, Livage J (1992) Aqueous chemistry of metal cations: hydrolysis, condensation and complexation. In: Reisfeld R, Jorgensen CK (eds) Chemistry, spectroscopy and applications of sol-gel glasses, Structure and bonding, vol 77. Springer-Verlag, Berlin, Heidelberg, pp 153–206

[16] Kocjan A, Krnel K, Kosmač T (2008) The influence of temperature and time on the AlN powder hydrolysis reaction products. J Eur Ceram Soc 28:1003–1008

[17] Kocjan A, Dakskobler A, KosmacÌŒ T (2012) Evolution of aluminum hydroxides in diluted aqueous aluminum nitride powder suspensions. Cryst Growth Des 12:1299–1307

[18] Kocjan A, Dakskobler A, Krnel K, Kosmač T (2011) The course of the hydrolysis and the reaction kinetics of AlN powder in diluted aqueous suspensions. J Eur Ceram Soc 31:815–823. doi:10.1016/j.jeurceramsoc.2010.12.009

[19] Dakskobler A, Kocjan A, Kosmač T (2011) Porous alumina ceramics prepared by the hydrolysis-assisted solidification method. J Am Ceram Soc 94:1374–1379. doi:10.1111/j.1551-2916.2010.04258.x

[20] Kocjan A, Ambrožič M, Kosmač T (2012) Stereometric analysis of nanostructured boehmite coatings synthesized by aluminum nitride powder hydrolysis. Ceram Int 38:4853–4859. doi:10.1016/j.ceramint.2012.02.075

[21] Kocjan A, Dakskobler A, Kosmac T (2011) Superhydrophobic nanostructured boehmite coatings prepared by AlN powder hydrolysis. Int J Appl Ceram Technol 8:848–853. doi:10.1111/j.1744-7402.2010.02516.x

[22] Jevnikar P, Krnel K, Kocjan A et al (2010) The effect of nano-structured alumina coating on resin-bond strength to zirconia ceramics. Dent Mater 26:688–696. doi:10.1016/j.dental.2010.03.013

[23] Wicklein B, Kocjan A, Salazar-Alvarez G et al (2015) Thermally insulating and fire-retardant lightweight anisotropic foams based on nanocellulose and graphene oxide. Nat Nanotechnol 10:277–283. doi:10.1038/nnano.2014.248

[24] Zhang S, Kocjan A, Lehmann F et al (2010) Influence of contamination on resin bond strength to nano-structured alumina-coated zirconia ceramic. Eur J Oral Sci 118:396–403. doi:10.1111/j.1600-0722.2010.00752.x

[25] Krokidis X, Raybaud P (2001) Theoretical study of the dehydration process of boehmite to γ-alumina. J Phys Chem B 105:5121–5130

[26] Okada K, Nagashima T, Kameshima Y, Yasumori A (2002) Effect of crystallite size on the thermal phase change and

porous properties of boehmite. J Colloid Interface Sci 248:111–115. doi:10.1006/jcis.2001.8183

[27] Klug HP, Alexander LE (1954) X-ray diffraction procedures for polycrystalline and amorphous materials, second. Wiley, New York

[28] Logar M, Kocjan A, Dakskobler A (2012) Photocatalytic activity of nanostructured γ-Al2O3/TiO2 composite powder formed via a polyelectrolyte-multilayer-assisted sol–gel reaction. Mater Res Bull 47:12–17. doi:10.1016/j.materresbull.2011.10.017

[29] Li M, Schnablegger H, Mann S (1999) Coupled synthesis and self-assembly of nanoparticles to give structures with controlled organization. Nature 402:393–395. doi:10.1038/46509

[30] Cai W, Yu J, Gu S, Jaroniec M (2010) Facile hydrothermal synthesis of hierarchical boehmite: sulfate-mediated transformation from nanoflakes to hollow microspheres. Cryst Growth Des 10:3977–3982. doi:10.1021/cg100544w

[31] Liu Y, Ma D, Han X et al (2008) Hydrothermal synthesis of microscale boehmite and gamma nanoleaves alumina. Mater Lett 62:1297–1301. doi:10.1016/j.matlet.2007.08.067

[32] Zhang L, Zhu Y-J (2008) Microwave-assisted solvothermal synthesis of AlOOH hierarchically nanostructured microspheres and their transformation to γ-Al2O3 with similar morphologies. J Phys Chem C 112:16764–16768. doi:10.1021/jp805751t

[33] Bowen P, Carry C, Luxembourg D, Hofmann H (2005) Colloidal processing and sintering of nanosized transition aluminas. Powder Technol 157:100–107. doi:10.1016/j.powtec.2005.05.015

[34] Sumirat I, Ando Y, Shimamura S (2006) Theoretical consideration of the effect of porosity on thermal conductivity of porous materials. J Porous Mater 13:439–443. doi:10.1007/s10934-006-8043-0

[35] Yang H-S, Bai G-R, Thompson LJ, Eastman JA (2002) Interfacial thermal resistance in nanocrystalline yttria-stabilized zirconia. Acta Mater 50:2309–2317. doi:10.1016/S1359-6454(02)00057-5

[36] Yu B, Lange F (2001) Colloidal isopressing: a new shape-forming method. Adv Mater 93106:276–280

[37] Romdhane M, Chartier T, Baklouti S et al (2007) A new processing aid for dry-pressing: a copolymer acting as dispersant and binder. J Eur Ceram Soc 27:2687–2695. doi:10.1016/j.jeurceramsoc.2006.11.076

[38] Zysset PK, Guo XE, Hoffler CE et al (1999) Elastic modulus and hardness of cortical and trabecular bone lamellae quantified by nanoindentation. J Biomech 32:1005–1012

[39] Burghard Z, Leineweber A, Van Aken PA et al (2013) Hydrogen-bond reinforced vanadia nanofiber paper of high stiffness. Adv Mater 25:2468–2473. doi:10.1002/adma.201300135

[40] Ohji T, Fukushima M (2012) Macro-porous ceramics: processing and properties. Int Mater Rev 57:115–131. doi:10.1179/1743280411Y.0000000006

[41] Konegger T, Patidar R, Bordia RK (2015) A novel processing approach for free-standing porous non-oxide ceramic supports from polycarbosilane and polysilazane precursors. J Eur Ceram Soc 35:2679–2683. doi:10.1016/j.jeurceramsoc.2015.03.009